Effect of Carbon Black and Silica Fillers in Elastomer Blends

Yimin Zhang,[†] S. Ge,[†] B. Tang,[†] T. Koga,[†] M. H. Rafailovich,*[,†] J. C. Sokolov,[†] D. G. Peiffer,[‡] Z. Li,[‡] A. J. Dias,[§] K. O. McElrath,[§] M. Y. Lin,[⊥] S. K. Satija,[⊥] S. G. Urquhart,[#,&] H. Ade,[#] and D. Nguyen[$]

Department of Materials Science and Engineering, State University of New York at Stony Brook, Stony Brook, New York 11794-2275; ExxonMobil Research and Engineering Company, Annandale, New Jersey 08801; ExxonMobil Chemical Company, Polymer Science and Butyl Technology Divisions, Baytown, Texas 77520; Center for Neutron Research, National Institute of Standards and Technology, Gaithersburg, Maryland 20899; Department of Physics, North Carolina State University, Raleigh, North Carolina 27695; and Brookhaven National Laboratory, Upton, New York 11973

Received January 30, 2001

ABSTRACT: The effects of carbon black and pyrogeneous silica fillers on the interfacial properties of a homopolymer [polybutadiene, (PB)] and a terpolymer [brominated poly(isobutylene-*co*-*p*-methylstyrene), (BIMS)] are reported. Neutron reflectivity (NR) was used to study the interfacial structure. The results are complemented by scanning transmission X-ray microscopy (STXM) and lateral force microscopy (LFM), which were used to probe the morphology and surface lateral force. Small-angle neutron scattering (SANS) was used to characterize the size and surface properties of the filler aggregates in elastomers. Our results show that the interfacial behavior of PB/BIMS is more sensitive to carbon black than to silica. The interfacial broadening is significantly slowed down with addition of merely $\phi_{CB} = 0.01$ (volume fraction) carbon black fillers. This volume level is much lower than that used in bulk rubbers ($\phi_{CB} \geq 0.1$). Pyrogeneous silica has a less pronounced effect on the interfacial characteristics. When both carbon and silica are incorporated into the PB layer, the effect of carbon black is offset by silica fillers.

Introduction

Fillers exist in a variety of systems such as organic, biological, biomimetic, and polymeric materials.[1] In the latter instance, the fillers are intentionally added. In polymer systems, fillers not only reduce the cost of the material but also improve the mechanical and dynamic properties of the compounds. Carbon black and silica are the most widely used fillers in rubber industry. For example, carbon black imparts strength and toughness to elastomers, improves the rubber's resistance to tearing, abrasion, and flex fatigue, and also increases traction and durability.[2] Silica and other types of fillers have a weaker polymer−filler interaction and are extensively used where a high degree of reinforcement is not essential.[3] Recently, silica was found to improve the processability of rubbers and was used as partial or even complete replacement for carbon black fillers.[4]

Consequently, a significant research effort was dedicated to explain the complex reinforcing effects of fillers in rubber matrices. Although there are disagreements in certain areas, it is well accepted that the reinforcement effects are due to molecular interactions of the rubber and filler particles.[5] Previous studies of filler−elastomer systems have mostly been conducted on bulk rubber with a large volume fraction ($\phi \geq 0.1$) of filler particles. For example, rheological data on filled compounds of varying filler volume fraction, such as Mooney viscosity, minimum torque of curometer measurement, and modulus, indicate that the reinforcing effect is not apparent unless the carbon black filler volume fraction is more than 0.05.

In many applications, different types of unfilled and filled rubber compounds are blended. The ultimate properties of these blends are directly related to the interfacial structure and properties. Control of the interfacial properties, such as adhesion, can have a dramatic impact on the performance of the blend. However, quantification of surface and interface properties is less explored due to the complexity of the polymer−filler matrix. Previously, several groups have shown that the dynamics of polymers near an attractive interface can be drastically reduced.[6−9] In a filler−polymer composite, especially in polymer nanocomposites, there is a large excess of interfacial area created. Hence, it is important to determine how the interfacial interactions between the filler and polymers affect the dynamics of interface formation and rheological properties.

The two elastomers studied in this work are polybutadiene (PB) and brominated poly(isobutylene-*co*-*p*-methylstyrene) (BIMS), a synthetic terpolymer of isobutylene (IB), *p*-methylstyrene (PMS), and *p*-bromomethylstyrene (BrPMS). The molecular structures of BIMS and its unbrominated analogue copolymer poly(isobutylene-*co*-*p*-methylstyrene) (IMS) are shown in Figure 1. Isobutylene-based elastomers are widely used in the automotive industry because these materials possess low permeability to gases, and one can control the mechanical properties by varying the level of IB and PMS as well as filler content and cross-link density.[10] Consequently, in standard rubber tires, both the hard sidewall and the softer inner liner can be made of carbon-reinforced BIMS blended with butyl and natural rubber.[11]

[†] State University of New York at Stony Brook.
[‡] ExxonMobil Research and Engineering Company.
[§] ExxonMobil Chemical Company.
[⊥] National Institute of Standards and Technology.
[#] North Carolina State University.
[$] Brookhaven National Laboratory.
[&] Current address: Department of Chemistry, University of Saskatchewan, Saskatoon, SK S7N 5C9, Canada.
* To whom correspondence should be addressed.

10.1021/ma010183p CCC: $20.00
Published on Web 08/31/2001

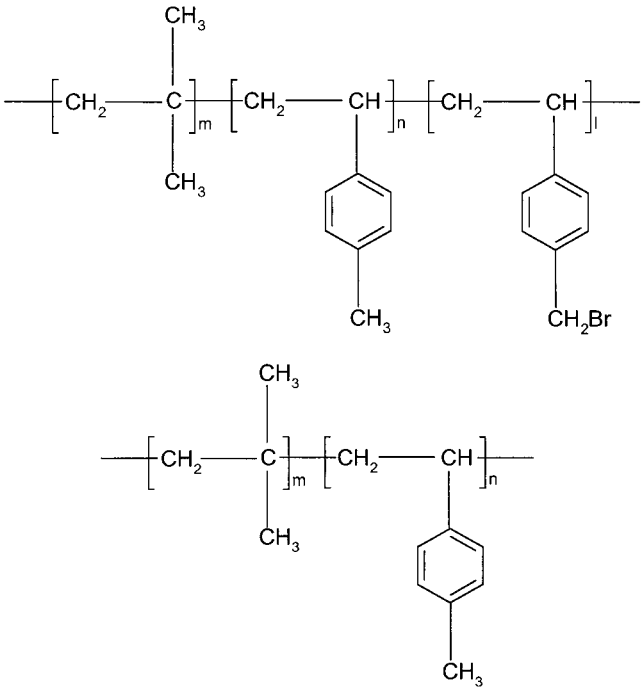

Figure 1. Molecular structures of the BIMS terpolymers and IMS copolymer.

Table 1. Isobutylene, *p*-Methylstyrene, *p*-Bromomethylstyrene, Number-Averaged Molecular Weight (M_n), and Neutron Scattering Length Density (SLD) of BIMS and IMS Polymers Used in This Study

polymer	PIB (mol %)	PMS (mol %)	BrPMS (mol %)	M_n (kg/mol)	SLD (10^{-6} Å^{-2})
BIMS-1	93	6.2	0.75	189	−0.21
BIMS-2	94	5.2	0.85	∼200	−0.23
BIMS-3	96	2.5	1.2	∼200	−0.27
IMS	94	6.1	0	∼200	−0.23

In this paper we describe neutron reflectivity (NR) measurements to determine the effects of low carbon black and silica filler fraction on the interface formation between BIMS and PB. Small-angle neutron scattering (SANS) is used to characterize the domain size of filler aggregates in elastomer−filler matrixes. Lateral force microscopy (LFM) and scanning transmission X-ray microscopy (STXM) are used to determine the surface rheological properties in the presence of fillers.

Experimental Section

Materials. The characteristic data of several grades of BIMS terpolymer and the unbrominated analogue copolymer (IMS), provided by ExxonMobil Chemical Corp. (Baytown, TX), are listed in Table 1. Both polymers are elastomeric in nature with a low T_g (−50 °C).[10] The polydispersity of these commercial polymers is in the range 2.5−2.8. Monodisperse dPB (M_n = 223 000, M_w/M_n < 1.03) was purchased from Polymer Source Inc., Montreal, Canada. Three types of carbon black, N330, N351, and N660, were supplied by Carbot Corp., Billerica, MA, with primary particle sizes of 290, 290, and 500 Å, respectively. Silica particles were pyrogenous silica Aerosil 300, with primary particle size of 90 Å and specific surface area of 295 m^2/g. The density of carbon black and silica are 1.85 and 2.2 g/cm^3, which was used for conversion from weight fraction to volume fraction (ϕ). Detailed characteristics of these fillers can be found elsewhere.[12,13] Hereafter, we use ϕ_{CB} and ϕ_{SF} to describe the volume fraction of carbon black and silica fillers, respectively.

Small-Angle Neuron Scattering (SANS). Prescribed amounts of carbon black and polymer, as listed in Table 2, were weighted and mixed in a Brabender at 100 rpm and 150 °C for 10 min. Approximately 0.5 g of the mixture was placed in a sample holder. The final shape of the sample is circular with a thickness of 1 mm with the flat faces perpendicular to the neutron beam. This path length was chosen to ensure the best balance between the scattering intensity and attenuation. Otherwise, the samples are considered isotropic with no preferred orientation.

Table 2. Composition and Aggregate Size of SANS Samples

polymer	vol fraction (ϕ) of filler	R_g of aggregates (Å)
IMS	ϕ_{CB} = 0.025	1200
IMS	ϕ_{CB} = 0.005	1200
BIMS-2	ϕ_{CB} = 0.025	1100
BIMS-2	ϕ_{CB} = 0.005	1100
BIMS-3	ϕ_{SF} = 0.025	>10000

To probe an extended range of the momentum transfer, or scattering wavevector, q, a combination of conventional SANS and ultrasmall-angle neutron scattering (USANS) measurements were performed. The conventional SANS was performed at the Center for Neutron Research (NCNR), the National Institute of Standards and Technology (NIST), in Gaithersburg, MD. A neutron wavelength of 6 Å was used, with two collimation configurations. One has a sample−detector distance of 2.9 m, measuring the high q range of 0.03−0.2 Å^{-1}. The other has the sample−detector distance set at 15.2 m, measuring a medium q range from 0.003 to 0.04 Å^{-1}. Standard samples were used to calibrate the instrument so all intensity measured was of the absolute scale of scattering cross section per unit volume (unit of cm^{-1}). The USANS experiments were performed at Oak Ridge National Laboratory, in Oak Ridge, TN. A Bonse-Hart setup with two triple bounce Si crystals was used as monochromator and analyzer for the ultrahigh angular resolution obtained.[14] With the neutron wavelength set at 2.59 Å, the instrument produces ultralow q range data of 0.0001−0.002 Å^{-1}. Because USANS data were taken with slit geometry and conventional SANS has pinhole geometry, a deconvolution was done for the USANS data before all three sets of the data from the same sample were merged, producing a wide q range from 0.0001 to 0.2 Å^{-1}.

Neutron Reflectometry (NR). A detailed procedure of sample preparation was described in a previous article.[15] Here we only briefly describe this procedure. The NR samples consist of two polymer layers. The first layer of dPB was spin-coated on silicon substrates from a toluene solution at 2500 rpm. To prepare analogue dPB layers with carbon black or hydrophobic silica fillers, the filler was weighted and dissolved in a small amount of toluene by sonication, and then the filler-containing solution was thoroughly mixed with a prescribed amount of the dPB solution before spin-coating. The silicon wafer substrate was 1 cm thick and 7.6 cm in diameter and was etched by HF to ensure a hydrophobic surface before introducing the first layer of dPB. This layer was then preannealed at 120 °C for 1 h in a vacuum of 10^{-3} Torr to relax any strains and remove the solvent introduced from the spinning process. The second layer was prepared by molding 5 g of BIMS (or carbon-filled elastomer of prescribed composition) into a disk-shaped piece, which has a thickness of 1 mm and a diameter of 7.6 cm. The two layers were sandwiched just prior to the NR experiment. To measure the interdiffusion between the two polymer layers, the bilayer sample, confined in a special press, was placed in an oven and annealed in a vacuum of 10^{-3} Torr at 150 °C for prescribed times. After annealing, the samples were quickly quenched in air to room temperature within 5 min.

The sandwiched wafers were then mounted on the horizontal sample table at the NIST neutron reflection spectrometer. The NR geometry is shown in Figure 2. The neutron beam enters through the 1 cm thick silicon wafer in the Q_{in} direction, and then it is reflected from the BIMS/dPB and silicon interfaces and is detected again in the Q_{out} direction. The technique of NR and its data analysis were previously discussed in a review by Russell.[16] In this work, there are seven

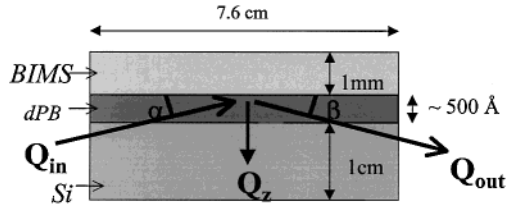

Figure 2. Typical geometry of specular neutron reflectivity setup. A thin dPB film is spun-cast onto a 1 cm thick Si wafer. A 1 mm thick disk of BIMS is placed on top of the dPB layer. The neutron beam enters through the Si wafer in the Q_{in} direction. The beam is reflected from the dPB/BIMS interface and is detected in the Q_{out} direction.

Table 3. Structure and Composition of Seven Bilayer Samples for NR Experiment

	lower dPB layer		top elastomer Layer	
sample designation	thickness (Å)	filler vol	elastomer	filler vol
A	500	0	BIMS-1	0
B	450	$\phi_{CB} = 0.003$	BIMS-1	0
C	380	$\phi_{CB} = 0.005$	BIMS-1	0
D	380	$\phi_{CB} = 0.025$	BIMS-1	0
E	580	0	IMS	$\phi_{CB} = 0.025$
F	600	$\phi_{SF} = 0.005$	BIMS-1	0
G	600	0	BIMS-2	$\phi_{CB} = \phi_{SF} = 0.01$

bilayer samples, the compositions of which are listed in Table 3. We will hereafter mention these bilayers as samples A−G.

Scanning Transmission X-ray Microscopy (STXM). The STXM samples were prepared by spin-coating films of approximately 1200 Å thick on Si_3N_4 membranes. The Si_3N_4 membrane provides an X-ray transparent substrate to support the thin polymer layers for X-ray microscopy investigation. The resultant two films (50/50 blend of dPB/BIMS-1 and 50/50 blend of PB/BIMS-1 with fillers $\phi_{CB} = 0.025$) were annealed in a vacuum oven for 18 h at 150 °C. The STXM experiment was performed on beamline X1A at the National Synchrotron Light Source (NSLS) at Brookhaven National Laboratory (BNL). The STXM microscope uses diffractive focusing optics (a Fresnel zone plate) to produce a microprobe with a 35−50 nm diameter. An image is formed by measuring the transmitted X-ray signal as a thin sample section (typically ∼100 nm thick) is raster scanned through the focus of the zone plate. The X-ray energy used for imaging can be chosen to correspond to discrete electronic transitions in the material, such as the C 1s → $\pi^*_{C=C}$ transition associated with C═C double bonds, which occurs at ∼285 eV in most materials. This X-ray absorption can be used to form a chemical image contrast. This microscope has been described by Jacobsen et al.,[17] and the applications to polymers were recently reviewed.[18]

Lateral Force Microscopy (LFM). Silicon wafers (300 μm thick, orientation 100, Wafer World Inc., West Palm Beach, FL) were cut into 2 cm × 2 cm pieces and cleaned by CrO_3/H_2SO4 solution followed by dilute HF to remove any organic and the oxide layer. The initially stationary wafer was flooded with toluene containing 14 mg/mL dPB and carbon black N330 of $\phi_{CB} = 0-0.15$ and then quickly (within 2 s) accelerated to 2500 rpm for 30 s. The resultant films, with thickness approximately 690 Å, were measured with a Rudolph AutoEL ellipsometer. The reference polystyrene (PS, M_n = 280K, Polymer Source Inc.) layers were first spin-coated onto glass substrates. After being floated off the glass substrates and onto the surface of a distilled water bath, the PS films were picked up by the silicon wafers precoated with carbon-black-filled dPB layers. The PS film is 230 Å thick and only partially covers the precoated dPB surface. Subsequently, the double-layer samples were dried in air for 24 h. The thin films with silica fillers were prepared by a similar procedure.

The topography and lateral force of these dPB layers containing different ϕ_{CB} and ϕ_{SF} were imaged with a DI3000 AFM (Nanoscope IIIa, Digital Instruments, Co., Ltd., Santa Barbara, CA). The AFM was operated in the contact mode, at room temperature, in a sealed glovebox purged with dry nitrogen gas, using a silicon nitride tip on a cantilever with a bending spring constant of 0.02−0.1 N/m. The image force was repulsive, approximately 25 nN. LFM images the lateral deflections of the cantilever from forces on the cantilever parallel to the plane of the sample surface. To obtain the maximum LFM signal, the cantilever was scanned along the direction perpendicular to its axis. The lateral force measurement investigates the friction variation of the elastomer surfaces. Since the true value of cantilever spring constant is unknown, the relative lateral force was estimated by using a reference PS layer covered on the sample surface.

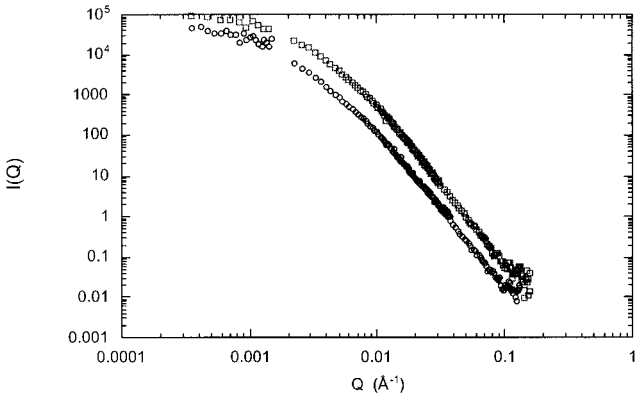

Figure 3. A log−log plot of scattering intensity (I) as a function of q for IMS blended with carbon N330 of $\phi_{CB} = 0.025$ (upper curve) and $\phi_{CB} = 0.005$ (lower curve).

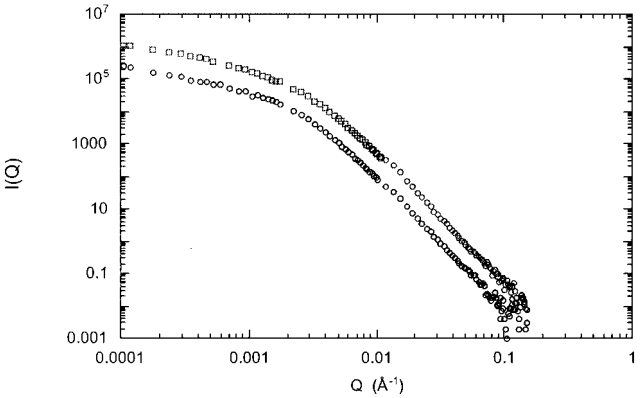

Figure 4. A log−log plot of scattering intensity as a function of q for BIMS-2 blended with carbon N660 of $\phi_{CB} = 0.025$ (upper curve) and $\phi_{CB} = 0.005$ (lower curve).

Results and Discussion

Small-Angle Neutron Scattering. SANS measures the micromorphology of a bulk sample. We combine conventional SANS and USANS to probe length scales from 10 Å to microns. Therefore, the purpose of SANS experiments was to observe whether the filler particles are well dispersed in the elastomer matrix and to characterize the size of filler particles or aggregates. In addition, interfacial properties between the particles and their surrounding polymer chains can also be probed with SANS.

The result of two slightly different systems, N330/BIMS-2 and N660/IMS, is shown in Figure 3 and Figure 4. In the figures we plot the scattering intensity I as a function of q. The two curves in each figure represent two different carbon/elastomer volume fractions (upper curves, $\phi_{CB} = 0.025$; lower curves, $\phi_{CB} = 0.005$) to test concentration effects, if any. The intensity for both samples scales with ϕ_{CB} (actual scaling not shown),

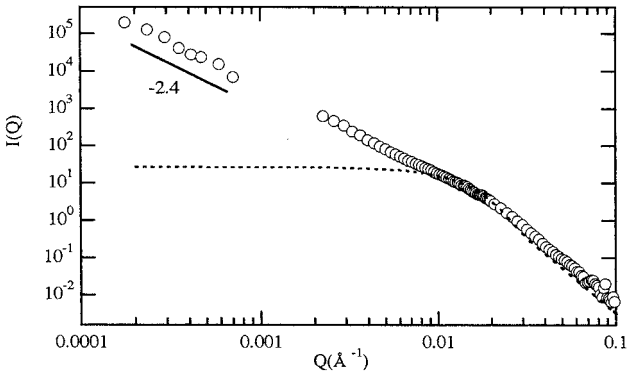

Figure 5. A log−log plot of scattering intensity as a function of q for BIMS-3 blended with hydrophilic silica $\phi_{SF} = 0.005$. At low q region "rollover" was not found. Dotted line is the best fit of spherical model to scattering profiles. The diameter, R, and polydispersity, $(\Delta R)/R$, of the particles are 90 Å and 0.3, respectively.

indicating little concentration effects. The combination of SANS and USANS data from $q = 0.0003$ to 0.2 Å^{-1} cover a very broad q range for the carbon black aggregates. A roll-over toward the low q end can be seen from the curves, allowing Guinier fits of the data to obtain the radius of gyration of the individual aggregates. Guinier's equation is as follows:[19]

$$I = I_0 e^{-(1/3)q^2 R_g^2} \quad (\text{if } qR_g \leq 1)$$

where I is the scattered intensity, I_0 is a q-independent quantity, and R_g is the average radius of gyration. Therefore, if $\ln(I)$ is plotted vs q^2 in the ultralow q range ($q < 0.001$ Å^{-1}), the slope of the linear fit equals $-1/_3 R_g^2$. It should be noted that this argument is valid only if there is a linear fit between the two quantities, and qR_g is smaller than or close to 1. Using this method, we obtained the R_g values of the two slightly different carbon/elastomer systems (1100 and 1200 Å), which were also listed in Table 2. On the basis of the primary particle size of 290 and 500 Å, we estimate that approximately 10−50 primary particles form an average aggregate in these systems.

Also for the carbon black samples, a power law behavior can be seen at high q range. Fits to the Porod form[20]

$$I = Aq^{-\alpha} \quad (\text{if } qR_g \gg 1)$$

reveal that the exponent for the power law is $\alpha = 4.03 \pm 0.05$, suggesting rather sharp surfaces of the particles.

In contrast, the low-q data for silica/BIMS-3 system (Figure 5) do not show a roll-over shape in the Guinier region, even at the USANS range approaching $q_{min} = 0.0001$ Å^{-1} or a length scale of $1/q = 1$ μm. Therefore, the size of the aggregates or agglomerates is likely larger than several microns. This is in agreement with the literature that silica fillers have much stronger interparticle interactions.[21] The broad shoulder peak which corresponds to the form factor of the primary particles appeared around $q = 0.01$ Å^{-1} . On the basis of the spherical model that takes the polydispersity of the particles into account, the size of the primary particle was estimated to be ∼90 Å with polydispersity of ∼30%, which is in good agreement with the manufacturer's specification. In addition, the reasonable straight-line shape of the curve at low q suggests a fractal structure within the aggregates or agglomerates,

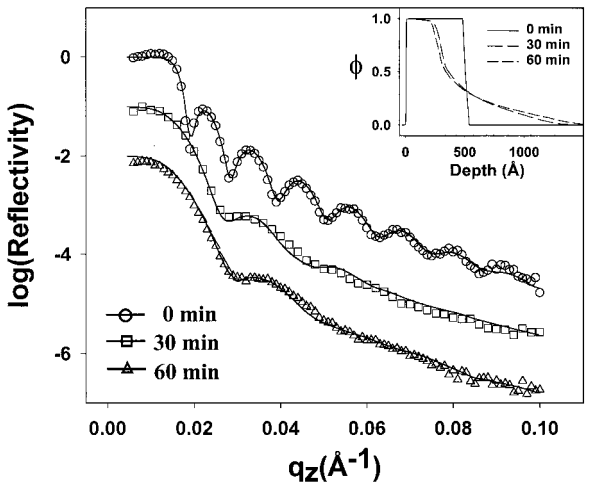

Figure 6. Neutron reflectivity data for different annealing times of the bilayer sample with a lower layer (dPB) 500 Å thick and an overlayer (BIMS-1) 1 mm thick. The solid lines represent the best fits to the experimental data. The data sets are offset for clarity. The inset shows best-fit profiles of dPB volume fraction as a function of distance from the silicon surface.

with a fractal dimension of $d_f = 2.41$. From the fitting at larger q, the curve bend to another power law, where the same Porod exponent is measured, $\alpha = 4.05 \pm 0.02$. As expected, both types of the filler particles do not fuse with the surrounding elastomers.

Neutron Reflectivity. All of the reflectivity profiles were plotted as log R vs Qz, where $Qz = (4\pi/\lambda) \sin \theta$, and Qz, λ, and θ are the incident neutron wave vector, neutron wavelength, and incident angle, respectively. For each sample, the reflectivity curves for different annealing times were vertically shifted in the same figure for clarity and comparison purposes.

Figure 6 shows the reflectivity profiles (R) obtained for sample A after annealing at 150 °C for 0 (i.e., no annealing), 30, 60, and 150 min. From the reflectivity curve for the unannealed sample we can see well-defined Kiessig oscillations, which indicate that the interface between the dPB layer and the BIMS-1 is sharp. The curve for the unannealed sample is fit by a single-layer model of dPB with an error function interface with the BIMS-1, which is assumed to be an infinite medium. The dPB layer is well fitted with a thickness of 494 Å and a dPB/BIMS interfacial width $w = 30$ Å, as shown in the inset. After annealing for 30 min, the amplitude of the oscillations decreases, indicating that the interface is becoming more diffuse. The concentration profile of diffused dPB layer can be fitted by an asymmetric model described elsewhere.[15] The dPB/BIMS interface after 30 min of annealing was found to be 260 Å. Further annealing for a total of 150 min yielded a profile with an interfacial width of 340 Å, which is in agreement with the equilibrium value measured previously.[15] The remaining low-frequency oscillation is due to a monolayer of dPB adsorbed to the hydrophobic silicon surface, which is discussed elsewhere.[15]

Figure 7 shows the reflectivity profiles for a sample where carbon black of $\phi_{CB} = 0.003$ was incorporated in the lower dPB layer (sample B). From the figure we can see that the interdiffusion has already begun to slow even though the carbon black concentration is very small.[22] The best fits to the data are shown in the inset where we can see that the interface gradually broadens

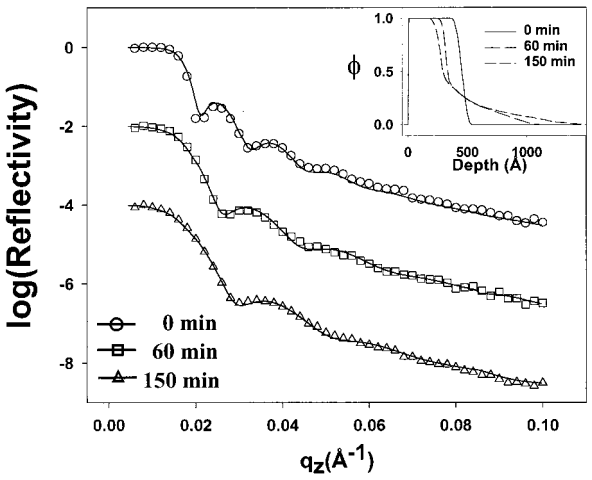

Figure 7. Neutron reflectivity data for different annealing times of the bilayer sample with a lower layer (dPB filled with carbon black N351 of $\phi_{CB} = 0.003$) 450 Å thick and an overlayer (BIMS-1) 1 mm thick. The solid lines represent the best fits to the experimental data. The data sets are offset for clarity. The inset shows best-fit profiles of dPB volume fraction as a function of distance from the silicon surface.

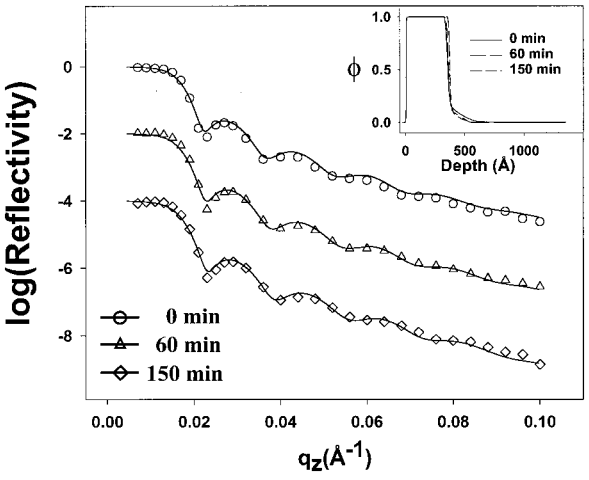

Figure 9. Neutron reflectivity data for different annealing times of the bilayer sample with a lower layer (dPB filled with carbon black N351 of $\phi_{CB} = 0.025$) 380 Å thick and an overlayer (BIMS-1) 1 mm thick. The solid lines represent the best fits to the experimental data. The data sets are offset for clarity. The inset shows best-fit profiles of dPB volume fraction as a function of distance from the silicon surface.

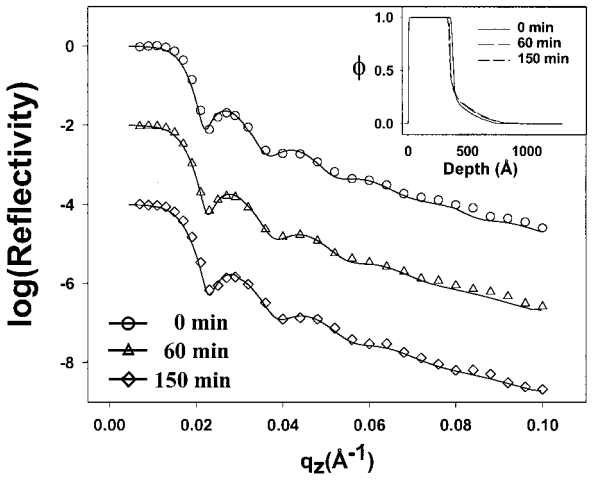

Figure 8. Neutron reflectivity data for different annealing times of the bilayer sample with a lower layer (dPB filled with carbon black N351 of $\phi_{CB} = 0.005$) 380 Å thick and an overlayer (BIMS-1) 1 mm thick. The solid lines represent the best fits to the experimental data. The data sets are offset for clarity. The inset shows best-fit profiles of dPB volume fraction as a function of distance from the silicon surface.

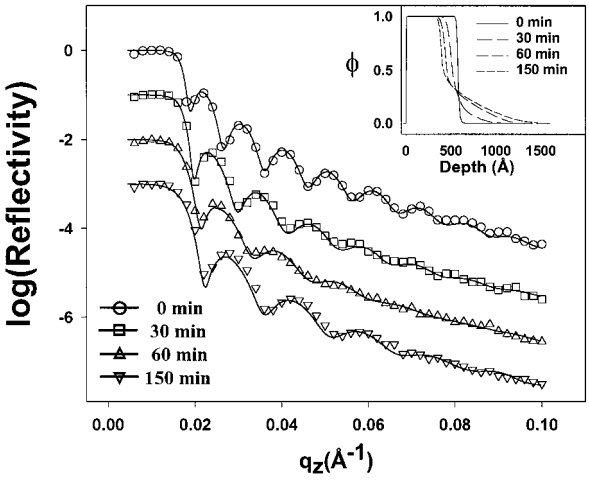

Figure 10. Neutron reflectivity data for different annealing times of the bilayer sample with a lower layer (dPB) 580 Å thick and an overlayer (IMS blended with carbon black N660 of $\phi_{CB} = 0.025$) 1 mm thick. The solid lines represent the best fits to the experimental data. The data sets are offset for clarity. The inset shows best-fit profiles of dPB volume fraction as a function of distance from the silicon surface.

from 50 Å for the unannealed sample to a maximum of 228 Å after annealing for 150 min. From Figure 8 we can see that when ϕ_{CB} is increased to 0.005 in the dPB layer (sample C), the interdiffusion is drastically slowed. The Kiessig oscillations in the specular reflectivity are hardly damped even after annealing at 150 ×bcC for 150 min. The volume profile that best fits the data is shown in the inset where we see that the interface broadens only from 30 to 50 Å after 150 min of annealing. When ϕ_{CB} is increased to 0.025 (sample D), interdiffusion was not observed at all. From the reflectivity data shown in Figure 9 we can see that the Kiessig oscillations are in fact slightly sharper in the annealed sample. The profiles used to fit the data are shown in the inset where we can see that the interface sharpens from 30 to 20 Å after annealing for 150 min. To rule out confinement effects in the thin dPB film or other interference from the proximity of the silicon interface, we also mixed carbon black particles into an IMS (i.e., the unbrominated analogue of BIMS) matrix using a Brabender mixer. In Figure 10 we show the reflectivity data for sample E which corresponds to an unfilled lower layer of dPB with a thickness of 580 Å sandwiched with a 1 mm thick slab of IMS with $\phi_{CB} = 0.025$. From the figure we can see that the Kiessig fringes persist after annealing for 150 min in this sample as well. From the profiles that are used to fit the data (shown in the inset) we can see that only a small amount of interdiffusion occurs. The interface shows a gradual broadening from 22 to 95 Å. Most of the broadening is due to a long tail in the fitted volume fraction profiles, probably induced by diffusion of the low molecular weight chains, as IMS and BIMS both have a relatively large polydispersity of 2.5−2.7. Hence, the addition of carbon black drastically slows down the interdiffusion regardless of the polymer matrix in which it is added. The quantities added are relatively small compared to the volumes usually added for commercial applications, such as

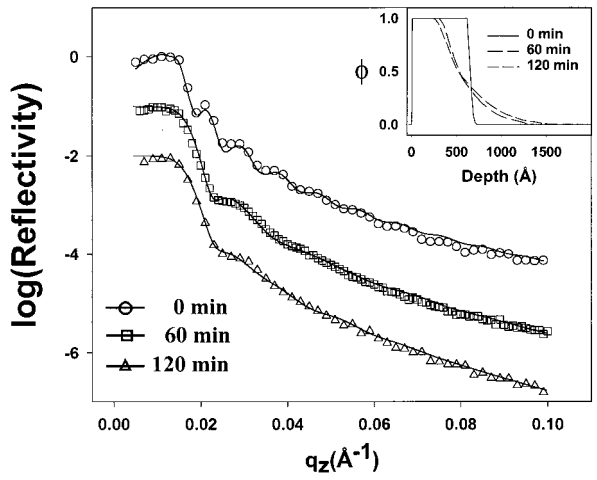

Figure 11. Neutron reflectivity data for different annealing times of the bilayer sample with a lower layer (dPB filled with silica of $\phi_{SF} = 0.005$) 600 Å thick and an overlayer (BIMS-1) 1 mm thick. The solid lines represent the best fits to the experimental data. The data sets are offset for clarity. The inset shows best-fit profiles of dPB volume fraction as a function of distance from the silicon surface.

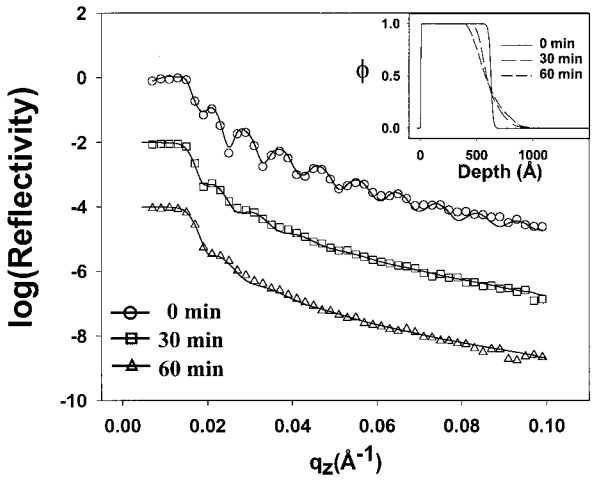

Figure 12. Neutron reflectivity data for different annealing times of the bilayer sample with a lower layer (dPB) 600 Å thick and an overlayer (BIMS-2 blended with $\phi_{CB} = \phi_{SF} = 0.01$) 1 mm thick. The solid lines represent the best fits to the experimental data. The data sets are offset for clarity. The inset shows best-fit profiles of dPB volume fraction as a function of distance from the silicon surface.

rubber tires and tire-forming bladders where the filler ($\phi_{CB} = 0.10-0.15$) is added for enhanced mechanical properties. To compare the effect of carbon black with silica fillers, hydrophilic silica of $\phi_{SF} = 0.005$ was incorporated into the dPB layer (sample F). The neutron reflectivity data are shown in Figure 11 where we see that the Kiessig oscillations are almost completely damped out after 60 min of annealing. Further annealing for a total of 120 min had only a modest effect on the interface dynamics. The inset shows that the interfacial width reached an "equilibrium" value of ~350 Å, which is close to that of the unfilled sample (A).

In many applications different fillers are blended together. An improvement in properties is found via this approach due to the possible interactions between the filler types. We therefore mixed two of the most common fillers, carbon black and silica of approximately $\phi = 0.01$ each, in the BIMS-2 layer, and sandwiched this layer with a 600 Å dPB layer (sample G). The neutron reflectivity data are shown in Figure 12. Despite the presence of the carbon black, the interface quickly reaches equilibrium, with w approximately 380 Å, as shown in the inset of Figure 12. Hence, the interfacial behavior of the mixed filler layer is characteristic of the silica filler rather than the carbon black filler.

Scanning Transmission X-ray Microscopy (STXM). To examine the effects of carbon black on the equilibrium phase morphology, symmetric blends of BIMS-1 and dPB without and with $\phi_{CB} = 0.025$ were spun-cast onto a Si_3N_4 membrane and annealed for 18 h at 150 °C. The STXM scans of the filled and unfilled samples are shown in parts a and b of Figure 13, respectively. The dark areas in the figure correspond to the intensity of the 285 eV π^*(C=C) absorption in dPB,[17] since the dPB phase contains a higher concentration of double bonds than the BIMS phase. From the figures we can see that dPB forms the continuous phase, while BIMS is the mostly discontinuous phase. Carbon black has a broad absorption band starting at ~284 eV; hence, these fillers can be imaged using an X-ray energy below the onset of the dPB absorption. However, only large aggregates of carbon black could be seen since the resolution of STXM microscopy was comparable to the

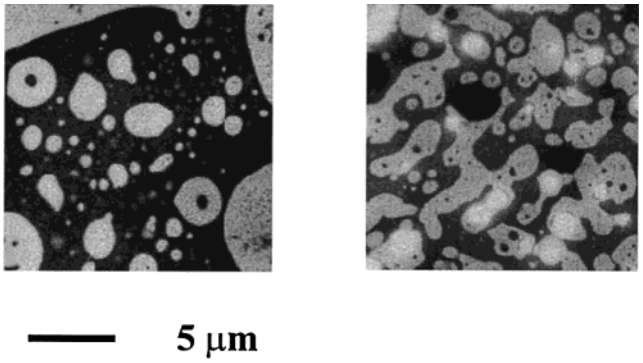

Figure 13. STXM scan (285 eV) of (a) 49/49/2 dPB/BIMS-1/carbon blend and (b) 50/50 dPB/BIMS-1 blend on Si_3N_4 membranes. Both films were annealed in a vacuum oven for 18 h at 150 °C. The dark areas correspond to the dPB phase.

size of the average carbon clusters as determined by USANS. Comparing the two figures, we see that the BIMS domains are taller and more discontinuous in the filled blend (Figure 13a) than in the unfilled blend (Figure 13b). Figure 14 is a scanning force microscopy image of the filled and unfilled blends of the same composition, annealed at 150 °C for 18 h. Comparing Figure 14 with the STXM image (Figure 13), we can see that the BIMS domains dewet the dPB surface in both blends. From the cross section analysis we obtain a contact angle of 10° and 6° between the BIMS-1 and dPB in the filled and unfilled blends, respectively. From these values we can estimate the equilibrium interfacial width to be 80 and 240 Å for the filled and unfilled systems.[23] These values are in very good agreement with the interfacial width obtained from the reflectivity data. Hence, the addition of small quantities of carbon black appears to inhibit interfacial mobility. The quantities of carbon black added should not alter the chemical nature of BIMS or dPB, and the quantities added are too small to cause an increase in the Flory–Huggins χ parameter. Hence, the observed effect is probably due to decreased dynamics within the polymer matrix caused by strong interactions between the polymer and the filler. These interactions are weakly present with silica fillers, and hence silica fillers do not perturb the

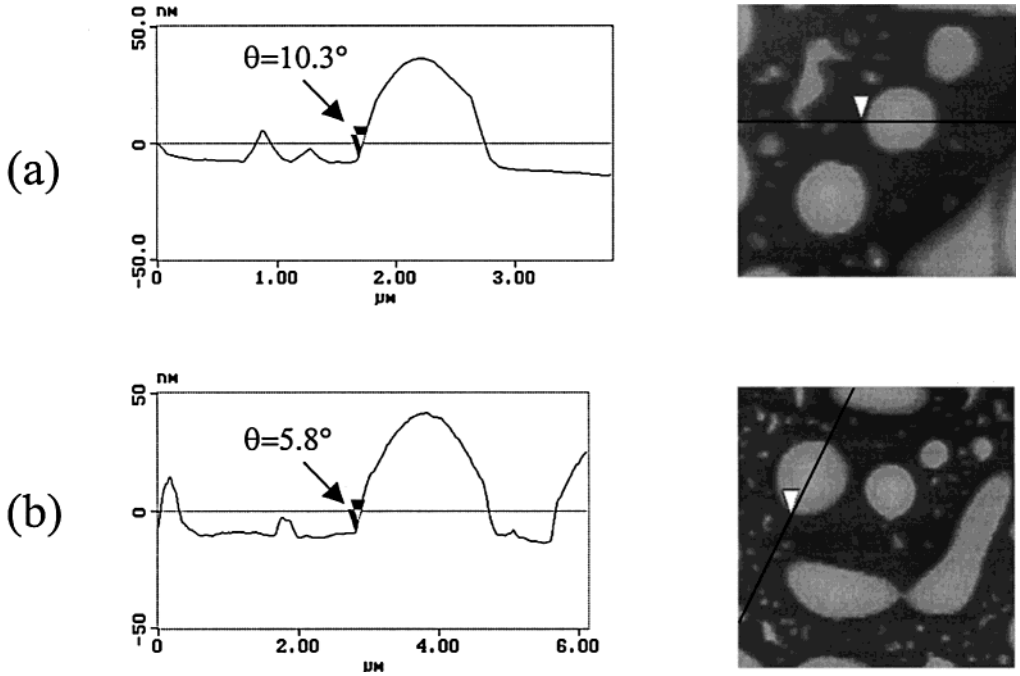

Figure 14. AFM image of an annealed BIMS-1/dPB (50/50) film of 500 Å (a) with carbon black filler $\phi_{CB} = 0.025$ (4 μm by 4 μm image) and (b) without carbon black filler (6 μm by 6 μm image).

internal dynamics. Unfortunately, it was not possible to continue annealing the NR samples in order to determine the ultimate interface since prolonged annealing of the bulk bilayer samples is not practical as degradation of the polymer may result, and the material begins to creep out of the sample holders.

Lateral Force Microscopy (LFM). A decrease in chain mobility induced by fillers should also reflect itself in the rheological properties of the filled homopolymers. Figure 15a−c shows the SFM and LFM images (left) of dPB films, approximately 690 Å thick, filled with increasing amounts of carbon black. The topmost figure corresponds to the unfilled dPB film. The lateral force loop corresponding to the deflection voltage in the cantilever trace and retrace signals of these images is shown on the right. From the lateral force loop of the unfilled sample we can see that the PS loop is much smaller than the dPB loop. The samples were scanned at room temperature, where the PS is glassy and high modulus (T_g = 100 °C), and hence the tip slips across the PS surface, producing a smaller frictional drag. The dPB layer, on the other hand, is an elastomer and relatively soft at room temperature (T_g = −20 °C), and hence the viscous drag on the tip is much larger. The magnitude of the lateral force is directly proportional to the deflection voltages where the proportionality constant is the spring constant of the cantilever. Since this value is not well characterized, we use the PS layer as a reference surface. If we assume the lateral force of PS (denoted as V_{PS}) to be a constant under the same experimental condition, the relative normalized force value (F_{dPB}, in arbitrary units) of the dPB surface equals the ratio of the two potentials, i.e., V_{dPB}/V_{PS}, where V_{dPB} and V_{dPB} are the deflection voltages of the cantilever in the dPB loop and PS loop, respectively. From Figure 15a we can see that F_{dPB} is typically much greater than 1 in the absence of filler. Figure 15b shows a dPB layer with ϕ_{CB} = 0.005. The lateral force loop on the right shows that F_{dPB} has begun to decrease. A few large aggregates have begun to appear on the surface, though most of the carbon is believed to be present as 100 nm particles, which are not visible with the AFM. Closer examination of Figure 15b shows that the aggregates appear much broader in the LFM than in topography images. The aggregates appear higher in the area covered by PS while their friction contrast is very low in the covered region. On the other hand, in the PB region we can see that the center of each aggregate is a low friction "hard" core surrounded by a large "corona" where the friction is higher than the surrounding background. This area extends over distances much larger than the topographical disturbance, indicating that the perturbation on the dynamics due to the particles can be long-ranged. Increasing the carbon black volume fraction to ϕ_{CB} = 0.025 (Figure 15c) further decreases the difference in the lateral force loop between V_{PS} and V_{dPB} until finally the two voltages are equal at ϕ_{CB} = 0.15. These results are summarized in Figure 16 where we plot F_{dPB} vs ϕ_{CB} or ϕ_{SF}. From the figure we find that the lateral force decreases with increasing ϕ_{CB} and reaches saturation at $\phi_{CB} \sim 0.05$. In addition, the silica filler reduces the lateral force, but to a lesser extent. The decrease in the lateral force indicates that dPB is becoming harder and more glassy in its rheological response to the moving tip. Clearly, carbon black has a more pronounced effect. These results are consistent with the slower dynamics observed for the same concentration range in the interfacial measurements.

In Figure 15d we also show the topographical and lateral force loop scans of dPB filled with hydrophilic silica particles of ϕ_{SF} = 0.025. From the figure we can see that the surface appears much smoother, and no large aggregates are present. The lateral force loop is seen to change only slightly with silica filler fraction. The lateral force vs ϕ_{SF} results are also plotted in Figure 16. From the figure we can see that the reduction of F_{dPB} as a function of ϕ_{SF} is much smaller than that of ϕ_{CB}. Furthermore, the decrease of F_{SF} with concentration is much more gradual, and saturation is not reached within the experimental concentration explored in this study, i.e., ϕ_{SF} = 0.15. Figure 15e shows the topography and lateral force scans of a dPB sample with

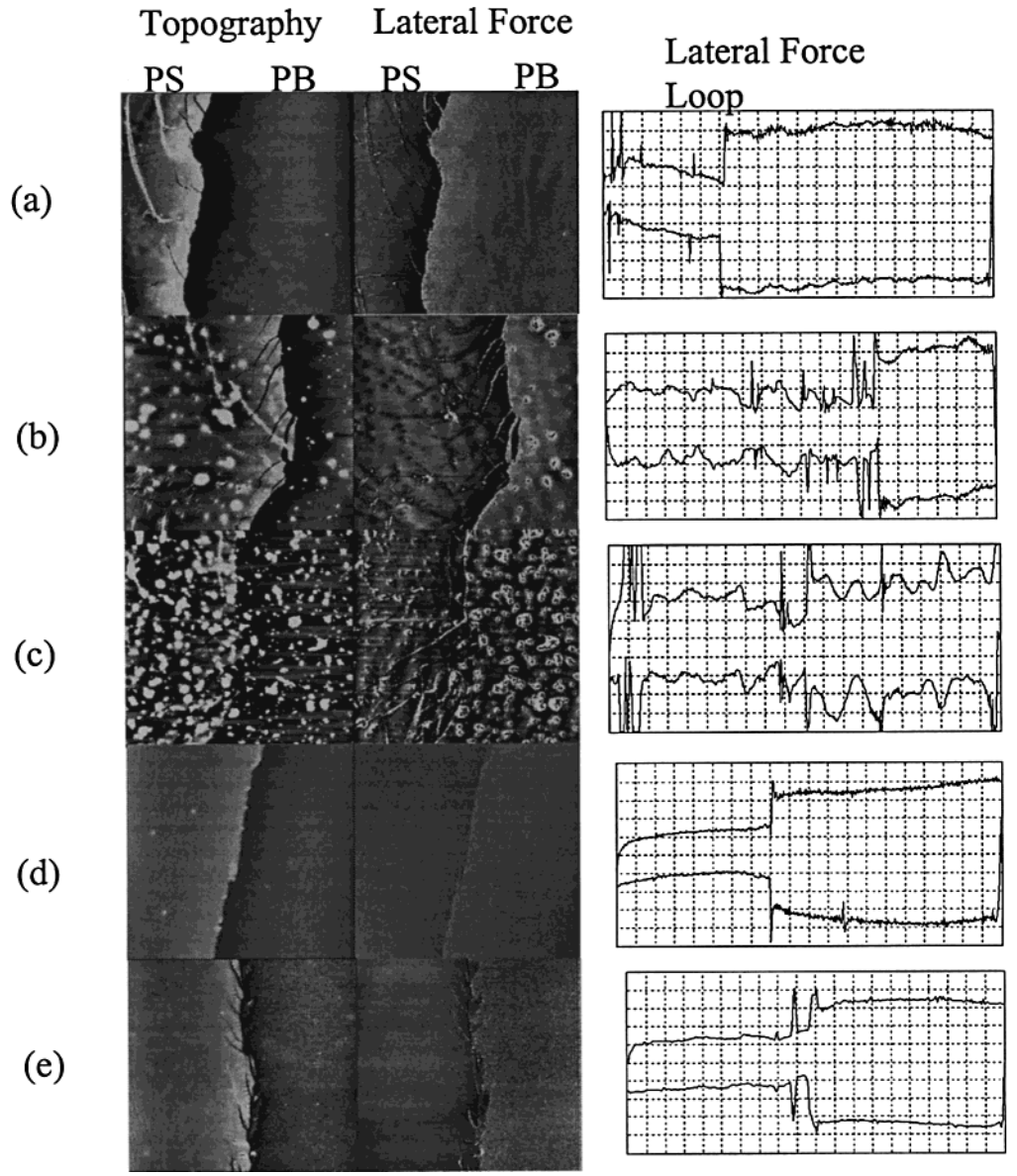

Figure 15. SFM (scanning force microscopy) and LFM (lateral force microscopy) images and lateral force loops of a 690 Å dPB film (a) without filler, (b) with $\phi_{CB} = 0.005$, (c) with $\phi_{CB} = 0.025$, (d) with $\phi_{SF} = 0.025$, and (e) with $\phi_{CB} = \phi_{SF} = 0.01$. A 230 Å PS layer partially covers the dPB surface.

carbon black and silica particle mixtures of $\phi_{CB} = \phi_{SF} = 0.01$. From the figure it is clear that the surface morphology as well as friction resembles that of the samples containing only silica even though the carbon black content is similar to sample Figure 15b. The relative friction of this sample is plotted as a triangle in Figure 16 where we can see that it overlaps the data points on the silica filler curve. These results are in agreement with the neutron reflectivity data which showed that the interfacial properties were more similar to the samples containing only the silica filler.

The effect of carbon black observed in both NR and AFM measurements can be attributed to the adsorption of the elastomer chains onto the filler particle surfaces. These adsorbed chains are usually described as "bound rubber" in the literature. Bound rubber was previously investigated and confirmed by extraction and atomic force microscopy.[24,25] These studies indicated that the dispersed filler particles act like a vulcanizing agent forming a "cross-linked" 3-dimensional elastomer network. In this network, each filler particle is adsorbed by a certain number of polymer chains. The number of bound chains is a function of the filler size and hence can vary for a given volume fraction of carbon black if agglomeration of the particles occurs. This model assumes that only chains in direct contact with the filler particles are immobilized.

The average interparticle distance T for a filler/polymer matrix may be estimated as follows:[26]

$$T = d[\beta(\pi/6\phi)^{1/3} - 1]$$

where d and ϕ are the average diameter and volume fraction of filler particles and β is a geometric constant close to 1. The values of the interpartical distance T as a function of volume fraction ϕ are plotted in Figure 17. Three curves for $d = 50$ nm (i.e., primary particle size of carbon black characterized by the manufacturer's TEM), $d = 120$ nm (i.e., USANS result for the average radius of gyration of the carbon aggregates in our samples), and $d = 0.5$ μm (i.e., minimum silica aggregate size) are shown in this figure. Both NR and

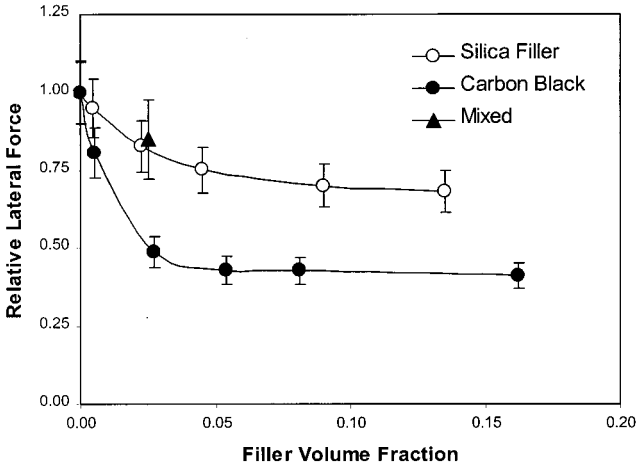

Figure 16. Relative friction of 690 Å thick filled-dPB film vs ϕ_{CB} and ϕ_{SF} in the dPB layer. The value of the sample with mixed fillers $\phi_{CB} = \phi_{SF} = 0.01$ is plotted as the filled triangle.

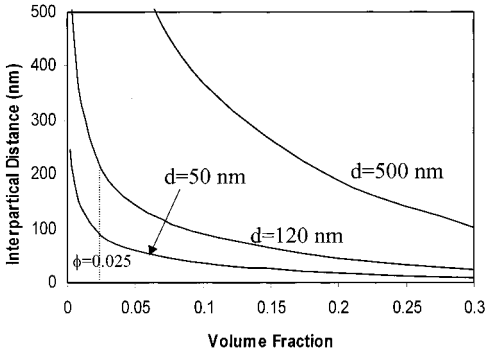

Figure 17. Interparticle distance (T) as a function of filler volume fraction (ϕ) for fillers with particle size (d) of 500 Å, 1200 Å, and 0.5 μm.

AFM indicate that the polymers behave as if they were cross-linked for $\phi_{CB} > 0.025$. At this volume fraction we can extrapolate from Figure 17 that the average interparticle distance is approximately 87 nm (for $d = 50$ nm) and 211 nm (for $d = 120$ nm). These values are significantly larger than the estimated size of the dPB chains ($R_g = 14$ nm). Since we do not see both a mobile and bound volume fractions of chains, we can conclude that the interaction between the particles and the elastomers are not limited to direct contact. It has been established by several groups that an attractive planar interface can drastically reduce the diffusion of polymer chains for distances on the order of 100 nm, or $10R_g$.[7,9,27] The nature of this long-range interaction is not well understood, but it is believed to be mediated by entanglements within the blend.[27] The planar interface has been approximated by a "two-fluid" model as illustrated in Figure 18a. One "fluid" is irreversible bound to the surface forming a densely cross-linked matrix (shown as green chains in Figure 18a), with a cross-linking density scaling as $N^{1/2} \ll N_e$, where N_e is the number of entanglements. Hence, chains trapped within this matrix (shown as blue chains in Figure 18a) are "strangulated" and diffuse much slower than the free chains (shown as red in Figure 18a) of the "bulk liquid".[28] It is reasonable to assume that a similar phenomenon also occurs in the vicinity of the attractive filler particles (Figure 18b). Hence, the filled system is the three-dimensional analogue of the planar thin-film samples. Following this analogy, the particles are covered by a bound layer of polymer (green chains) which then traps subsequent layers (blue chains) and hinders their diffusion. Only the layers in direct contact are irreversibly bound and detected by solvation methods described in the literature.[29] The other layers are entropically bound within the melt network but are easily removed with solvent.

When the attractive surface is covered by organic surfactants, as in the case of pyrogeneous silica fillers, where only van der Waals interactions within the polymer are present, it was shown that a much smaller decrease in the polymer dynamics occurs.[7] In addition, the range of the interaction is much shorter and affects only chains in direct contact with the surface. Even though the bare silicon surface is known to interact strongly with PB,[30] the surfactant used to disperse the colloidal silica fillers can screen the surface interaction. Hence, only a small effect on the dynamics is observed

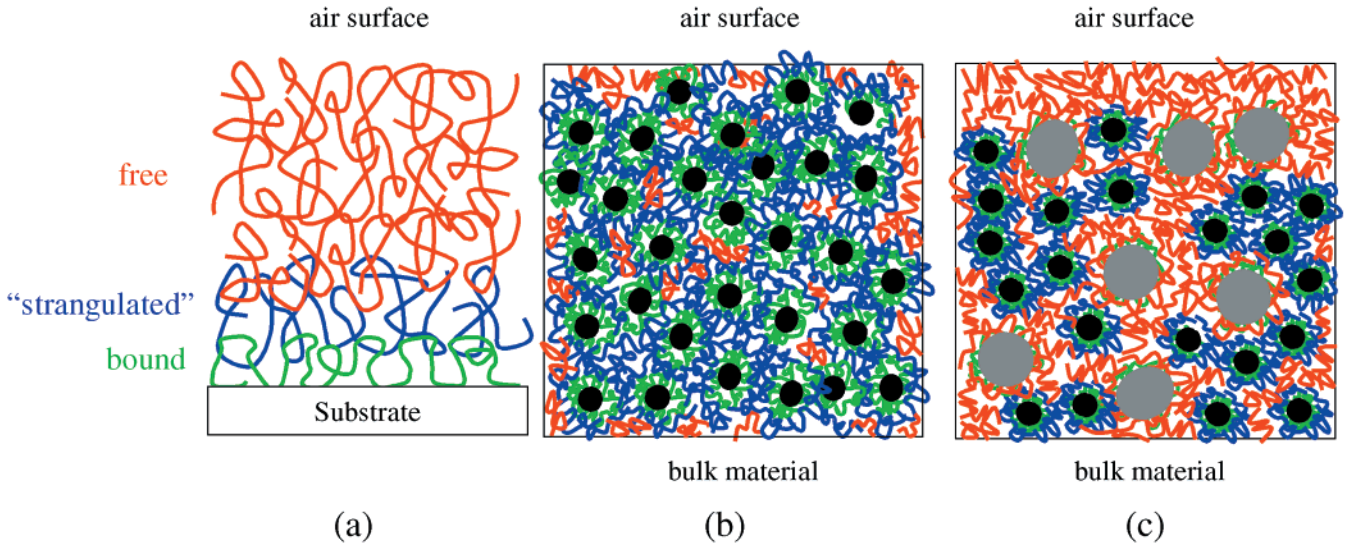

Figure 18. Schematic drawings of the polymer chain structure in (a) an elastomer thin film on a flat attractive substrate, (b) a section of a carbon-filled elastomer, and (c) a section of an elastomer with mixed carbon black and colloidal silica fillers. The "bound", "strangulated", and "free" chains are shown as green, blue, and red chains. The carbon and colloidal silica aggregates are designated by small and large spheres, respectively. Note that the size of the silica relative to carbon is reduced by a factor of 2 in order to show the segregation of elastomer chains at the free surface.

even though the filler volume fraction used is similar to those of carbon black. Furthermore, as can be seen from Figure 17, if the silica agglomerates are in excess of 0.5 μm, then the interparticle distance is too large to affect the overall dynamics.

It is interesting then to speculate as to what is occurring in the samples when the two fillers are mixed. The SANS data on bulk samples where carbon and silica filler were mixed with BIMS show a high scattering intensity which is comparable to that of the samples with only carbon black fillers.[31] Since it is not possible to distinguish which filler produces the scattering, we can only state that the number of scatterers is similar to that of the pure carbon black samples, which indicates that the carbon black fillers do not form large aggregates with the silica such as those reported where the two fillers were premixed without polymer.[29,32]

We suspect that in the mixed filler systems polymer chains bound to carbon black particles are trapped (shown as green) or have hindered mobility (shown as blue) whereas the chains in the vicinity of the colloidal silica fillers behave in a manner similar to "free" polymer (shown as red). The proposed model is shown in Figure 18c. The carbon filler acts as an effective "cross-linking" agent of the polymer due to the strong interaction with the chains. When colloidal silica filler is present, we assume the silica and carbon black aggregates are randomly situated in the bulk polymer matrix. It is entirely possible that if a silica aggregate is within a few chain dimensions, i.e., R_g, then less of the polymer matrix can interact with the carbon black surface, which essentially releases these chains from the constraints imposed on it by the more strongly interacting surface (Figure 18c). The free chains are then entropically excluded from the matrix and migrate to the free surface or interfaces in analogy to the segregation observed of homopolymer in a cross-linked matrix.[33]

Conclusions

We successfully measured the interdiffusion dynamics between two dissimilar elastomers by the neutron reflectivity technique. Strong adsorption of elastomer chains to carbon black particles is indirectly observed by both neutron reflectivity and LFM techniques. Calculation of the critical volume fraction indicates the polymer/filler interaction is long range. "Percolation" was therefore observed at ϕ_{CB} much below the amount used in the industry. LFM measurement on the surfaces of filled dPB films shows an increase in viscosity with as little as $\phi_{CB} = 0.005$ filler. The increase saturates at a volume fraction of $\phi_{CB} = 0.025$. Weaker confinement effects, i.e., interfacial narrowing or viscosity increase, were observed with either NR or LFM for systems filled with pyrogeneous silica. This was attributed to screening of the polymer/filler surface interactions by the surfactants used to stabilize the particles. When both carbon and silica were incorporated into the dPB layer, both the surface viscosity and the interfacial broadening were similar to the samples filled with only pyrogeneous silica. This was attributed to segregation of the "free polymer" and associated silica particles to the surface and interfaces. This is analogous to the segregation of free homopolymer from a cross-linked network, which in this case is formed by the physical cross-links of polymers adsorbed to attractive carbon black particles.

Acknowledgment. This work was supported by NSF MRSEC program. H.A. and S.G.U. are supported by NSF Young Investigator Award DMR-9458060.

References and Notes

(1) Ahmad, Z.; Mark, J. E. *Mater. Sci. Eng., C* **1998**, *6* (2−3), 183.
(2) Koenig, J. L. *Acc. Chem. Res.* **1999**, *32*, 1.
(3) Mark, J. E.; Erman, B.; Eirich, F. R. *Science and Technology of Rubber*, 2nd ed.; Academic Press: New York, 1994; p 388.
(4) Schaal, S.; Coran, A. Y.; Mowdood, S. K. *Rubber Chem. Technol.* **2000**, *73*, 240.
(5) Mori, M.; Koenig, J. L. *J. Appl. Polym. Sci.* **1998**, *70*, 1391.
(6) Frank, B.; Gast, A. P.; Russell, T. P.; Brown, H. R.; Hawker, C. *Macromolecules* **1996**, *29*, 6531.
(7) Zheng, X.; Rafailovich, M. H.; Sokolov, J.; Strzhemechny, Y.; Schwarz, S. A.; Sauer, B.; Rubinstein, M. *Phys. Rev. Lett.* **1997**, *79*, 241.
(8) Lin, E. K.; Kolb, R.; Satija, S. K.; Wu, W. L. *Macromolecules* **1999**, *32*, 3753.
(9) Buenviaje, C.; Ge, S.; Rafailovich, M. H.; Sokolov, J.; Drake, M.; Overney, R. *Langmuir* **1999**, *15*, 6446.
(10) Wang, H. C.; Powers, K. W. *Elastomerics* **1992**, February, 22.
(11) Gursky, L. J.; Fusco, J. V.; Flowers, D. D. U.S. Patent 5,532,312, 1996.
(12) Turov, V. V.; Leboda, R.; Bogillo, V. I.; Skubiszewska-Zieba, J. *Langmuir* **1995**, *11*, 931.
(13) Pieker, T. P.; Hindermann-Bischoff, M.; Ehrburger-Dolle, F. *Langmuir* **2000**, *16*, 5588.
(14) Agamalian, M.; Wignall, G.; Triolo, R. *Neutron News* **1998**, *9*, 24.
(15) Zhang, Y. et al., data submitted to *Polymer*.
(16) Russell, T. P. *Mater. Sci. Rep.* **1990**, *5*, 171; *Physica B* **1996**, *221*, 267.
(17) Jacobsen, C.; Williams, S.; Anderson, E.; Brown, M. T.; Buckley, C. J.; Kern, D.; Kirz, J.; Rivers, M.; Zhang, X. *Opt. Commun.* **1991**, *86*, 351.
(18) Ade, H.; Urquhart, S. G. In *Chemical Applications of Synchrotron Radiation*; Sham, T. K., Ed.; World Scientific Publishing, in press.
(19) Guinier, A.; Fournet, G. *Small Angle Scattering of X-rays;* John Wiley: New York, 1955.
(20) Porod, G. *Small-Angle X-ray Scattering*; Academic Press: New York, 1982.
(21) Donnet, J. B. *Rubber Chem. Technol.* **1998**, *71*, 323.
(22) Our experimental results indicated that the three types of carbon black, N330, N351, and N660, have little difference in affecting the diffusion properties. Therefore, we only show the results of N351 in the following experiments.
(23) Clark, C. J.; Eisenburg, A.; LaScala, Rafailovich, M.; Sokolov, J.; Li, Z.; Qu, S.; Nguyen, D.; Schwarz, S.; Strzhemechny, Y.; Sauer, B. *Macromolecules* **1997**, *30*, 4184.
(24) Gessler, A. M.; Hess, W. M.; Medalia, A. I. *Reinforcement of elastomers with carbon black, Plastics and Rubber: Processing* **1978**, Dec, 141.
(25) Niedermeier, W.; et al. *Kautschuk Gummi Kunststoffe* **1995**, *48*, 611.
(26) Wu, S. *J. Appl. Polym. Sci.* **1988**, *35*, 549.
(27) Wu, W. L.; Wallace, W. E.; van Zanten, J. H.; Bauer, B. J.; Liu, D. W.; Wong, A. *Polymer* **1997**, *38*, 2583.
(28) De Gennes, P. G. *Macromolecules* **1986**, *19*, 1245.
(29) Hamed, G. R. *Rubber Chem. Technol.* **2000**, *73*, 524.
(30) Zhao, W.; Rafailovich, M.; Sokolov, J.; Fetters, L.; Plano, R.; Sanyal, M.; Sinha, S.; Sauer, B. *Phys. Rev. Lett.* **1993**, *70*, 2659.
(31) Lin, M. Y. Data deferred for publication.
(32) Murphy, L. J.; Wang, M. J.; Mahmud, K. *Rubber Chem. Technol.* **2000**, *73*, 25.
(33) Jinnai, H.; Hasegawa, H.; Hashimoto, T.; Briber, R. M.; Han, C. C. *Macromolecules* **1993**, *26*, 182.

MA010183P